NISTIR 6496

Heat Transfer of Supercritical Carbon Dioxide Flowing in a Cooled Horizontal Tube

Douglas A. Olson

U.S. DEPARTMENT OF COMMERCE
Technology Administration
Process Measurements Division
Chemical Science and Technology Laboratory
National Institute of Standards and Technology
Gaithersburg, MD 20899

NIST
National Institute of Standards and Technology
Technology Administration
U.S. Department of Commerce

NISTIR 6496

Heat Transfer of Supercritical Carbon Dioxide Flowing in a Cooled Horizontal Tube

Douglas A. Olson

U.S. DEPARTMENT OF COMMERCE
Technology Administration
Process Measurements Division
Chemical Science and Technology Laboratory
National Institute of Standards and Technology
Gaithersburg, MD 20899

May 2000

U.S. DEPARTMENT OF COMMERCE
William M. Daley, Secretary

TECHNOLOGY ADMINISTRATION
Dr. Cheryl L. Shavers, Under Secretary of Commerce for Technology

NATIONAL INSTITUTE OF STANDARDS AND TECHNOLOGY
Raymond G. Kammer, Director

CONTENTS

LIST OF TABLES

LIST OF FIGURES

NOMENCLATURE

A_f	=	flow normal area for CO_2
A_{ht}	=	heat transfer area between the water and carbon dioxide, based on the inner tube inside radius
c_p	=	specific heat
D	=	diameter
f	=	friction factor
h	=	heat transfer coefficient
h_{CO2}	=	carbon dioxide heat transfer coefficient
h_{H2O}	=	water heat transfer coefficient
i	=	specific enthalpy at location L or 0 for water or CO_2
k	=	thermal conductivity
k_{ss}	=	thermal conductivity of the stainless steel of the tube
L	=	heat transfer length
m_{CO2}	=	carbon dioxide mass flow rate
m_{H2O}	=	water mass flow rate
n	=	exponent in Nu_{SCb} correlation
Nu	=	Nusselt number = hD/k
Nu_{CPb}	=	Nusselt number using constant property correlation, properties evaluated at T_b
Nu_{CPw}	=	Nusselt number using constant property correlation, properties evaluated at T_w
Nu_{SCb}	=	Nusselt number using supercritical heating correlation, properties evaluated at T_b
Nu_{SCw}	=	Nusselt number using supercritical cooling correlation, properties evaluated at T_w
Nu_{meas}	=	measured Nusselt number
p	=	exponent in Nu_{SCw} correlation
P	=	pressure
P_c	=	critical pressure
Pr	=	Prandtl number = $\mu c_p/k$
q	=	exponent in Nu_{SCw} correlation
Q	=	total heat transferred between the water and carbon dioxide over the entire heat exchanger length
Q_A	=	heat flux = Q/A_{ht}
Q_{CO2}	=	heat absorbed by the carbon dioxide in the heat exchanger
Q_{err}	=	error in heat balance
Q_{H2O}	=	heat released by the water in the heat exchanger
Q_{loss}	=	heat loss from water through tube insulation to the room
r_i	=	inner tube inside radius
r_o	=	inner tube outside radius
Re	=	Reynolds number = $\rho VD/\mu$
T	=	temperature
T_b	=	bulk fluid temperature, taken as average of CO_2 inlet and outlet temperatures
T_c	=	critical temperature
T_{CO2}	=	carbon dioxide temperature
T_{H2O}	=	water temperature
T_m	=	pseudocritical temperature, *i.e.,* temperature for which the specific heat is a maximum for the given pressure

T_w = wall temperature at the location of bulk temperature T_b
U = overall heat transfer coefficient
Uh_{CO2} = combined standard uncertainty in CO_2 heat transfer coefficient
Uh_{H2O} = combined standard uncertainty in water heat transfer coefficient
$U\Delta T_{LM}$ = combined standard uncertainty in log mean temperature difference
UNu_{meas} = combined standard uncertainty in measured Nusselt number
UPr_{CO2} = combined standard uncertainty in CO_2 Prandtl number
UQ_{CO2} = combined standard uncertainty in CO_2 heat flow
UQ_{err} = combined standard uncertainty in heat balance error
UQ_{H2O} = combined standard uncertainty in water heat flow
URe_{CO2} = combined standard uncertainty in CO_2 Reynolds number
V = velocity
W = mass flux = m/A_f

ΔP = pressure drop
ΔT_L = T_{H2O} - T_{CO2} at the "L" location of the heat exchanger, which is the CO_2 outlet and the water inlet
ΔT_{LM} = log mean temperature difference
ΔT_0 = T_{H2O} - T_{CO2} at the "0" location of the heat exchanger, which is the CO_2 inlet and the water outlet
μ = viscosity
ρ = density

Heat Transfer of Supercritical Carbon Dioxide Flowing in a Cooled Horizontal Tube

Douglas A. Olson
Process Measurements Division
National Institute of Standards and Technology
Gaithersburg, MD 20899

Abstract

We report measurements of heat transfer coefficients of flowing supercritical carbon dioxide (7.38 MPa critical pressure, 31.1 °C critical temperature) in a cooled horizontal tube. The tube was 10.9 mm ID, was cooled over 274 cm, and had an adiabatic entrance section of 55.9 cm. Cooling was accomplished by flowing cold water countercurrent to the carbon dioxide in an annular gap between the inner tube (12.7 mm OD) and an outer tube (16.6 mm ID). This set a convective boundary condition similar to what would be encountered in a counterflow heat exchanger. The four experimental parameters found to affect the heat transfer coefficients, and their ranges tested, were: operating pressure (7.409 MPa to 13.0 MPa), CO_2 mass flow rate (1.1 kg/min to 5.0 kg/min), rate of heat removal by cooling (1780 W to 6220 W), and CO_2 average temperature (4.3 °C below to 24.2 °C above the pseudocritical temperature). The Reynolds number range at the CO_2 average temperature was 63 250 to 291 700. Conditions which resulted in the highest heat transfer coefficients were pressure close to the critical, high mass flow rate, and temperature close to the pseudocritical. For CO_2 average temperatures lower than 1 °C below the pseudocritical, higher rates of cooling increased the heat transfer coefficient, whereas for temperatures higher than 1 °C below the pseudocritical, higher rates of cooling reduced the heat transfer coefficient. The measured Nusselt numbers were predicted to within experimental uncertainty by the Krasnoshchekov-Protopopov correlation for supercritical flow, when the CO_2 average temperature was above the pseudocritical. This correlation was developed for constant heat flux heating instead of cooling. No existing correlation was found to predict the measured Nusselt number when the CO_2 average temperature was lower than the pseudocritical. The measured heat transfer coefficients were higher than those predicted by the constant property correlations throughout the range of parameters tested.

Key words: carbon dioxide; cooled supercritical flow; counterflow heat exchanger; heat transfer; horizontal tubes; supercritical fluids; turbulent flow

---

Certain commercial equipment, instruments, materials, or software are identified in this paper to foster understanding. Such identification does not imply recommendation or endorsement by NIST, nor does it imply that the materials or equipment identified are necessarily the best available for the purpose.

1. Introduction

Carbon dioxide has been proposed as a "natural refrigerant" in various kinds of refrigeration, air conditioning, and heat pump cycles (Lorentzen and Pettersen, 1993). For equivalent cycle efficiencies, carbon dioxide offers much reduced ozone depletion potential and global warming potential than chlorofluorocarbons and hydrofluorocarbons. It is also non-toxic and non-flammable. However, system designs will have to be adapted to the characteristics of carbon dioxide, and the cycle efficiency will be important in determining whether the systems will be commercially viable. In contrast to cycles with conventional refrigerant fluids, the pressure in a carbon dioxide cycle will be above the critical during the heat rejection process. Hence a supercritical cooling operation would replace the gas condenser. Very little is known about the heat transfer of supercritical fluids undergoing cooling.

In this work we have measured the heat transfer performance of supercritical carbon dioxide that is cooled while flowing in a horizontal tube. (The carbon dioxide critical pressure, P_c, is 7.38 MPa and the critical temperature, T_c, is 31.1 °C). In this experiment, carbon dioxide at pressures higher than the critical flowed through a 10.9 mm ID tube and was cooled by water flowing countercurrent to it over 2.74 m of its length. The flow of CO_2 was turbulent throughout the tube. The primary experimental parameters that we varied were system pressure, flow rate, cooling rate, and temperature. We report how the heat transfer varies with the experimental parameters, and compare the data to correlations in the literature. This work is a companion experiment to the one we reported earlier (Olson and Allen, 1998). In that experiment, we measured heat transfer with supercritical carbon dioxide in the same tube, but the tube was heated instead of cooled by flowing water. Taken together, these results are a comprehensive description of the heat transfer in a supercritical fluid that exchanges heat with a secondary fluid.

Although heat transfer in supercritical fluids has been studied by many investigators, as summarized by Hall and Jackson (1978), nearly all of this work has been for flows undergoing heating. As pointed out by Pitla *et al.* (1998), the few correlations that exist for cooling situations show significant inconsistencies. Supercritical flows are complex because of the rapid variations in transport and thermophysical properties that occur near the critical point (Fig. 1; data from Span and Wagner, 1996, and Vesovic *et al.*, 1990). When heat transfer measurements are compared to those expected for a constant property fluid with these fluid properties, the heat transfer can be enhanced or degraded, depending on flow or heating conditions that have no effect in a constant property fluid. Our earlier work (Olson and Allen, 1998) showed that a correlation developed for supercritical flows undergoing constant wall heating can be used successfully when the boundary condition is a convective one. These results showed that both the heat flux and the system pressure cause the heat transfer of a supercritical fluid to deviate from that of a constant property fluid.

2. Description of experimental apparatus

2.1 Flow loops

Experiments were conducted with the counterflow heat exchanger test section placed in the heat transfer facility shown schematically in Figs. 2 and 3. The facility consists of two closed fluid

loops, one for carbon dioxide and one for water, which join at the test section. The flow loops were filled with instrument grade carbon dioxide (99.99 % purity) and deionized water, respectively.

Flow was circulated through the carbon dioxide loop by a centrifugal pump with a magnetically coupled drive, which had a maximum capacity of 72 L/min (at no pressure drop). A variable speed drive on the motor of the pump was used to control the flow rate. Carbon dioxide was added to the system with a 500 mL syringe pump, which also controlled the operating pressure. Flow rate was measured with a coriolis flow meter. After exiting the flow meter, the carbon dioxide entered an "electric heater" heat exchanger, which raised its temperature to the desired test section inlet temperature, about 89 °C at the maximum. The electric heater consisted of 5.5 m of 19.1 mm OD 316 stainless steel tubing, wrapped on the outside with a 9 kW heater coil. The heater coil was powered by a 208VAC, 50 amp SCR controlled power supply. Setting the power to the coil controlled the temperature of the carbon dioxide leaving the heater section. Upon exiting the heater section, the carbon dioxide entered the test section, which was a counterflow heat exchanger with cold water flowing in the annular gap outside of the tube containing the carbon dioxide. After leaving the test section, the carbon dioxide was cooled down to ambient temperature by another counterflow heat exchanger, referred to as the "gas cooler", utilizing laboratory cold water as the cold sink. This heat exchanger contained 5.5 m of 12.7 mm OD tubing for the heat exchange area. The carbon dioxide then reentered the pump. The system volume was about 2 L. The tubing connecting the test section outlet to the gas cooler was 19 mm OD 316 stainless steel, and the tubing from the heater to the test section inlet connection was a Teflon-lined, stainless steel braided hose. All of the remaining tubing was 12.7 mm OD 316 stainless steel. All components in the flow loop were rated to a pressure of 13.8 MPa or higher.

The water flow loop was similar in design to the carbon dioxide flow loop. The water was circulated with a turbine pump, rated for 19 L/min at 40 m of head. The flow rate was controlled with the pump bypass valve. Flow rate was also measured with a coriolis flow meter. After exiting the flow meter, the water entered the "primary cooler". The primary cooler was a counterflow heat exchanger containing 5.5 m of 19 mm OD stainless steel tubing, with laboratory chilled water (5 °C) as the cold sink. The flow rate of the chilled water to the primary cooler could be controlled from 0 to 15 L/min. The flow loop water entered the "secondary cooler" after leaving the primary cooler. This heat exchanger also contained 5.5 m of 19 mm OD stainless steel tubing, with a 60/40 mixture of ethylene glycol/water flowing countercurrent to the water. The temperature of the glycol/water mixture was controlled by pumping it from a recirculating cooler (3 kW capacity at 0 °C, controllable temperature). Setting the flow rate of the chilled water to the primary cooler, in combination with the temperature of the glycol/water mixture in the recirculating cooler, controlled the temperature of the water entering the test section. The carbon dioxide in the test section then heated the water. An air-operated piston pump was used to fill the flow loop and maintain pressure when the system was operating. A back-pressure regulator prevented over-pressure of the system due to thermal expansion of the water. The water loop was rated to pressures up to 2100 kPa, and was operated at about 700 kPa. All connecting tubing was 19.1 mm OD, 316 stainless steel.

The electric heater of the carbon dioxide loop was insulated with 2.5 cm of basalt-fiber insulation

overlaid with 1.3 cm of fiberglass pipe insulation. The connecting tubing between the electric heater and the test section was insulated with 1.3 cm of fiberglass pipe insulation. The gas cooler and all remaining connecting tubing in the carbon dioxide loop were insulated with 1.3 cm of neoprene insulation. The primary and secondary coolers of the water flow loop were insulated with 1.3 cm of neoprene insulation. All of the connecting tubing of the water flow loop was insulated with 1.3 cm of fiberglass insulation.

2.2 Test section

The experimental test section is shown in Fig. 4. It was a counterflow heat exchanger consisting of a 12.7 mm OD, 10.9 mm ID inner tube mounted concentric to a 19.1 mm OD, 16.6 mm ID outer tube. Carbon dioxide flowed from left-to-right inside the inner tube, and water flowed from right-to-left in the annular space (1.9 mm radial gap) between the two tubes (as per Fig. 4). The tubes were mounted at both ends in O-ring compression fittings that sealed the carbon dioxide and permitted axial movement due to thermal expansion. These fittings were coupled to swaged fittings in which the flow loop inlet and outlet tubing was connected. The length of the inner tube was 348 cm. The first 55.9 cm of tubing was surrounded by insulation only, and hence there was no heat transfer. The outer tube, from centerline to centerline of the connection fittings, extended over the next 274.3 cm of the inner tube. The final 17.8 cm of the inner tube length also was insulated only. The length-to-diameter ratio of the entrance section was 51 (based on the inner tube inner diameter), and the length-to-diameter ratio of the heated section was 251.

The inlet and outlet temperatures of the carbon dioxide and the water to the test section were measured in thermowells (made from commercially available 3/4 inch "T" fittings) that permitted the insertion of the thermometers and allowed the fluid to flow past the thermometers. The test section outlet thermowells were located a minimum of 15 cm from the last 90° bend to the test section, which provided sufficient tube length to mix the fluids to a uniform temperature. Pressure taps were located in the carbon dioxide flow loop at the thermowells. Pressure taps were located in the water flow loop a short distance upstream of the test section inlet and downstream of the outlet. The inlet pressure of both loops was connected to absolute pressure transducers, and the pressure difference between the inlets and outlets was measured with differential pressure transducers. The entire test section was mounted on a rigid aluminum I-beam. Slotted holes with Teflon shims provided axial movement of the test section relative to the I-beam, which resulted from thermal expansion. The test section was insulated with 1.3 cm thick fiberglass pipe insulation, as were all the thermowells, thermometers, and connecting tubing from the flow loops.

2.3 Instrumentation

We measured the mass flow rate, test section inlet temperature, test section outlet temperature, test section inlet pressure, and test section differential pressure for both the carbon dioxide and water sides of the test section. Both of the mass flow rates were measured with coriolis mass flow meters. The carbon dioxide flow meter had a range of 0 kg/min to 10 kg/min, with a manufacturer's stated relative uncertainty of ± 0.15 % of reading, ± 0.68 kg/h zero stability. The water flow meter had a range of 0 kg/min to 30 kg/min, with a manufacturer's stated relative

uncertainty of ± 0.10 % of reading, ± 0.163 kg/h zero stability. (For this and other manufacturer's stated uncertainties, we assume the values given are normal distributions and that they have about a 95 % "confidence interval". Hence the "standard uncertainty" is ½ the stated value. See Taylor and Kuyatt [1994] for a detailed description of the NIST uncertainty policy).

We measured fluid temperatures with platinum resistance thermometers, 6.4 mm diameter and 15 cm long. The probes were calibrated by the manufacturer and had a combined repeatability and hysteresis uncertainty of ± 0.05 °C. The probe measuring the carbon dioxide inlet temperature was immersed to a depth of 5.1 cm; the remaining probes were immersed to a depth of 7.6 cm. Self-heating and stem conduction errors were calculated to be less than ± 0.001 °C. The carbon dioxide pressure at the test section inlet was measured with a quartz crystal pressure transducer with a 41 MPa full scale range. The combined repeatability, linearity, and hysteresis uncertainty of the transducer was ± 4.1 kPa. Water absolute pressure, water differential pressure, and carbon dioxide differential pressure were measured with variable-reluctance pressure transducers. These transducers each had a combined repeatability, linearity, and hysteresis uncertainty of ± 0.25 % of full scale; or an absolute uncertainty of 5200 Pa, 860 Pa, and 86 Pa, respectively for the water absolute pressure, water differential pressure, and carbon dioxide differential pressure.

Signals from the thermometers and variable reluctance pressure transducers were multiplexed through an automated scanner and measured with a digital voltmeter. Signals from the flowmeters were measured with a frequency counter. The signal from the quartz crystal pressure transducer was converted to an ASCII character string by the manufacturer's electronics. Relay switching transients and voltmeter A/D conversion introduced negligible uncertainty in the measured quantities. Measurement of the signals was controlled by a personal computer. Raw signals and converted parameters were stored on the hard drive. Some of the parameters were displayed on the video monitor to assist in monitoring and operating the experiment. Heat transfer performance parameters were calculated at the completion of the experiments.

3. Description of experiments and analysis techniques

3.1 Experiments conducted and procedure

Seven "data sets" of experiments were conducted and their conditions are summarized in Table 1. Each set was performed on a separate day. The major conditions that were varied for the set are shown in bold typeface. The pressure throughout the test section was above the critical for all experiments. For data sets 1 through 4, the carbon dioxide pressure was fixed at a constant value, while the carbon dioxide flow rate and the cooling heat transfer rate were varied. Typically, four cooling rates were tested at five flow rates each. For these four data sets we also held the average of the carbon dioxide inlet and outlet temperatures (T_b) approximately constant at 1 to 2 °C above T_m. The pseudocritical temperature, T_m, is the temperature at the operating pressure where the specific heat reaches its maximum (slightly above the critical temperature), and as the results which follow will show, it is an important parameter in determining the heat transfer performance. For four of the 79 settings, the T_b-T_m temperature difference exceeded 2 °C. This occurred at high cooling rates and low CO_2 flow rates, and was due to the minimum temperature possible in the water loop (9 °C).

In data set 5, the CO_2 pressure was varied at constant flow rate and several values of the cooling rate. The pressure was decreased to within 0.3 % of the critical. The average CO_2 temperature was kept approximately constant, which resulted in changes in T_b-T_m as the pressure varied. In data set 6, the pressure was held constant at 7.8 MPa, the flow rate was kept constant, and the average temperature was varied for several cooling flow rates. Finally, in data set 7, we varied the flow rate and heating rate at constant pressure, this time with the average temperature colder than T_m.

Once a setting was achieved, the instruments were scanned and signals stored multiple times (usually 11). All of the measured and calculated values for each scan of the instruments, each experimental setting, can be found as Excel 2000 files on the diskette in the back cover on the report. Altogether we achieved 142 experimental settings and sampled 1564 data points. Measured parameters are listed first, followed by calculated performance parameters, and finally standard uncertainties of the most important parameters. For the first 8 settings of data set 3, the water pressure drop was not measured. It was estimated based on the flow rate and density.

We filled the carbon dioxide loop in a consistent manner to achieve a high purity of carbon dioxide. Beginning with air at atmospheric pressure in the system, the loop was pressurized with carbon dioxide gas at the saturation pressure of the supply bottles (about 5.7 MPa). This mixture of air and carbon dioxide was vented down to a pressure slightly above atmospheric, preventing back-filling with air. The procedure of filling with carbon dioxide and venting to atmosphere was performed a minimum of three times. Assuming uniform mixing of the initial charge and the added carbon dioxide during each fill, this reduced the air concentration to a volume fraction of less than 1×10^{-6}. After the fourth fill of carbon dioxide gas, we filled the syringe pump with liquid carbon dioxide from a bottle containing a dip tube. The pump dispensed the liquid into the flow loop. The syringe pump was re-filled from the bottle and the liquid dispensed into the loop until the loop pressure began to increase, indicating all the vapor space was filled with liquid. Using the syringe pump in a constant pressure mode set the system pressure. Prior to circulating the carbon dioxide and starting heat transfer, the syringe pump was set at about half-full. This allowed it to both dispense and withdraw fluid as the specific volume of carbon dioxide in the flow loop changed due to temperature changes.

To generate heat exchange between the carbon dioxide and the water in the heat exchanger test section, both circulating pumps were turned on. The gas cooler in the CO_2 loop was turned on to maintain a high density in the fluid entering the pump. Turning on and adjusting the power to the electric heater increased the temperature of the carbon dioxide. Heat was removed from the water and its temperature was adjusted by: (1) turning on the lab chilled water flow to the primary cooler; and (2) setting the temperature of the recirculating cooler which pumped coolant to the secondary cooler. In some cases, settings which required high water temperatures allowed us to shut off the secondary cooler. For some settings at low cooling rates, we could turn off the primary cooler and use the secondary cooler by itself. The four major independent parameters, which allowed setting the conditions for an experiment, were the power to the CO_2 electric heater, the recirculating cooler temperature, the carbon dioxide flow rate, and the carbon dioxide pressure. We adjusted the heater power and the recirculating cooler temperature until the carbon dioxide average temperature and heat transferred achieved the desired values.

Achieving a new steady setting after any of the four parameters were changed required about 15 min. Large changes in temperature required more time, and small temperature changes or small flow rate changes required less time. We defined this stability as a condition when the changes of the experimental parameters or measured quantities with respect to time were small enough so that negligible errors were introduced into the calculated performance parameters (< 0.1%). Flow and pressure steady state occurred within seconds of changing the set point, whereas thermal steady state required temperatures of the electric heater, recirculating cooler, and test section to stabilize. Observing the temperature changes at the fluid thermometers indicated thermal stability. A drift rate of 0.1 °C/min was low enough to introduce negligible error in the performance parameters.

3.2 Analysis to determine heat transfer coefficient

We characterized the heat transfer performance of the supercritical carbon dioxide by calculating the heat transfer coefficient from the experimental data. The heat exchanger test section had three major modes of heat transfer: convection from the hot carbon dioxide to the inner wall; radial conduction through the tube wall; and convection from the inner tube to the water. The basic principle of the data analysis was to calculate the overall heat transfer performance and then subtract out the tube conduction and water convection to get the carbon dioxide performance. Axial conduction in the tube and two fluids was insignificant. Conduction out the insulation to the ambient room was a few percent and was accounted for in calibration.

Heat transfer in a counterflow heat exchanger can be expressed by the "log mean temperature difference" equation which *defines* the overall heat transfer coefficient, U (Rohsenow and Choi, 1961):

$$Q = UA_{ht}\Delta T_{LM}\,, \tag{1}$$

where

$$\Delta T_{LM} = \frac{\Delta T_L - \Delta T_0}{\ln \dfrac{\Delta T_L}{\Delta T_0}}\,.$$

Here,
- Q = total heat transferred between the water and carbon dioxide over the entire heat exchanger length;
- A_{ht} = heat transfer area between the water and carbon dioxide, based on the inner tube inside radius;
- U = overall heat transfer coefficient;
- T = temperature, either water (H_2O) or carbon dioxide (CO_2);
- ΔT_{LM} = log mean temperature difference;
- ΔT_L = T_{CO2} - T_{H2O} at the "*L*" location of the heat exchanger, which is the CO_2 outlet and the water inlet; and
- ΔT_0 = T_{CO2} - T_{H2O} at the "*0*" location of the heat exchanger, which is the CO_2 inlet and the water outlet.

If the overall heat transfer coefficient is constant throughout the heat exchanger, then we can derive Eq. (1) by integrating the local differential heat flux equation from end to end. Because the transport properties of the carbon dioxide are temperature dependent, the local carbon dioxide heat transfer coefficient will vary in the heat exchanger, and U defined in Eq. (1) will not always equal the local value. The local heat flux will also vary along the tube length.

U can be further decoupled into the carbon dioxide convection, tube conduction, and water convection components through the assumption of linear addition of the heat transfer modes:

$$\frac{1}{U} = \frac{1}{h_{CO2}} + \frac{r_i}{k_{ss}} \ln \frac{r_o}{r_i} + \frac{r_i}{r_o} \frac{1}{h_{H2O}}, \tag{2}$$

where h_{CO2} = carbon dioxide heat transfer coefficient;
r_i = inner tube inside radius;
k_{ss} = thermal conductivity of the stainless steel of the tube;
r_o = inner tube outside radius; and
h_{H2O} = water heat transfer coefficient.

The tube radius multipliers account for the different heat transfer area for the three terms. We note that Eq. (2) defines both h_{CO2} and h_{H2O} as "average" coefficients that are a single value for the entire tube length. In order to determine h_{CO2} as a function of position along the tube, we would need to know the heat flux as a function of position, or the specific enthalpy of either the water or carbon dioxide as a function of position. The value of h_{H2O} was measured in the apparatus prior to performing the experiments of this report, by operating the test section with hot water in the inner tube and cold water in the annular gap. h_{H2O} was a function of water flow rate and temperature, which was accounted for in its experimentally derived correlation equation. Typical values were 7000 to 11 000 W/(m^{2}K).

We calculated Q from the measurements of the heat released by the flowing carbon dioxide and the heat absorbed by the water:

$$Q = Q_{CO2} = m_{CO2}(i_0 - i_L)_{CO2}, \tag{3}$$

$$Q = Q_{H2O} = m_{H2O}(i_L - i_0)_{H2O} + Q_{loss}, \tag{4}$$

where m_{CO2} = carbon dioxide mass flow rate (measured);
m_{H2O} = water mass flow rate (measured);
i = specific enthalpy at location L or 0 for water or CO_2; and
Q_{loss} = heat loss from water through tube insulation to the room.

The specific enthalpy was calculated from thermodynamic equations of state for the water and carbon dioxide at the measured temperature and pressure, P:

$$i = i(T, P). \tag{5}$$

The equation of state of Span and Wagner (1996) was used for the carbon dioxide, and the NIST Steam Tables were used for water (Gallagher and Haar, 1988). Q_{loss} was measured as a function of water temperature by operating the water flow loop without carbon dioxide cooling ($Q_{H2O} = 0$ in Eq. (4)). It ranged from 0 % to 6 % of Q, and in some cases was negative when the water was colder than ambient.

To determine h_{CO2} at each test point, the heat flow was calculated from the measured temperatures, pressures, and flow rates using Eqs. (3), (4), and (5). Q_{H2O} was used in Eq. (1) along with the measured temperatures to calculate U. The value of h_{CO2} was then calculated from Eq. (2) by subtracting the tube conduction and water convection terms from U.

In the results that follow in Sec. 4, we present h_{CO2} as a function of the average heat flux and the carbon dioxide mass flux. Their definitions are:

$$Q_A = Q/A_{ht} = \text{heat flux;} \tag{6}$$

$$W = m/A_f = \text{mass flux.} \tag{7}$$

A_f is the flow normal area for the CO_2. We also calculated the Nusselt number (Nu), along with the Reynolds number (Re) and Prandtl number (Pr) for the carbon dioxide at each test condition.

$$Nu = \frac{hD}{k}, \tag{8}$$

$$Re = \frac{\rho VD}{\mu}, \tag{9}$$

$$Pr = \frac{\mu c_p}{k}, \tag{10}$$

where k = thermal conductivity;
V = velocity;
ρ = density;
c_p = specific heat; and
μ = viscosity.

Because the temperature of the carbon dioxide changed from the inlet to the outlet and from the tube center to the wall, the fluid properties also changed throughout the flow. The fluid properties were evaluated at T_b (the average of the CO_2 inlet and outlet) in the data analysis. The density and specific heat were calculated from Span and Wagner (1996), while the viscosity and thermal conductivity were calculated from Vesovic *et al.* (1990). The functions of Vesovic *et al.* include the enhancement of both the thermal conductivity and the viscosity around the critical point.

3.3 Experimental uncertainty

A summary of the standard and combined standard uncertainties is listed in Table 2. Uncertainties in the carbon dioxide property functions and equation of state were taken as ± 4 % at the 95 % confidence interval, based on Vesovic *et al.* (1990) and Span and Wagner (1996). Combined standard uncertainties in the calculated quantities, such as Q, U, h_{CO2}, Nu, Re, and Pr, were calculated using the "law of propagation of uncertainty" as stated in Taylor and Kuyatt (1994). This method involves writing a Taylor series approximation of those quantities and applying the partial derivatives of the quantity with respect to each variable times the standard uncertainty of the variable. Derivatives of the thermodynamic and transport properties were approximated with finite differences.

Multiplying the values in the Table by a coverage factor of 2 gives a 95 % confidence interval that the actual uncertainty is less than or equal to the stated uncertainty. The Table also lists the major sources of uncertainty for each parameter. We can evaluate the quality of the measurements by comparing the combined standard uncertainty of the heat balance error (Q_{H2O}-Q_{CO2})/Q_{CO2} to the experimentally measured heat balance error, Q_{err}. The experimental Q_{err} ranged from –40 % to +8.8 %. Settings where the heat balance error was larger than ±5 % corresponded to conditions with either the inlet or outlet CO_2 temperature within 0.2 °C of T_m. Because of the high specific heat at T_m, the uncertainty in the measured temperature produced a large uncertainty in the enthalpy and therefore the CO_2 heat flow at those settings. Twice the calculated standard uncertainty closely mirrored the measured Q_{err} for those settings. If we eliminate 12 of the 142 settings with the inlet or outlet temperatures close to T_m, twice the calculated standard uncertainty in Q_{err} is 4.1 % to 9.4 %. For those 130 settings, the measured Q_{err} ranges from –4.7 % to +4.3 %, with a standard deviation of 1.0 %. Because the measured uncertainties in Q_{err} are less than or equal to twice the calculated standard uncertainties, we are confident that we have estimated the measured uncertainties properly, and that the uncertainties for the remaining calculated quantities have been estimated conservatively. We have used Q_{H2O} for Q in Eq. (1) due to the error produced by the uncertainty in the measured CO_2 temperature on the CO_2 enthalpy.

Combined standard uncertainties in h_{CO2} ranged from 1.3 % when the magnitude of h_{CO2} was low, to 9.8 % when its magnitude was high. The largest source of the uncertainty in h_{CO2} was the uncertainty in h_{H2O}; at high values of h_{CO2} the uncertainty in h_{CO2} was magnified by the ratio of h_{CO2}/h_{H2O} due to the subtraction of the water-side heat transfer from the overall measured heat transfer (Eq. 2). The combined standard uncertainty in Nu_{meas} ranged from 2.4 % to 10.1 %.

4. Results of experiments

4.1 Effects of experimental parameters on heat transfer coefficient

Effect of W, Q_A, and P with $T_b > T_m$. The measured heat transfer coefficient, h_{CO2}, for the supercritical carbon dioxide from data sets 1 to 4 is plotted in Figs. 5 to 7. For all of these data sets, the average temperature, T_b, is greater than T_m. The figures show representative data points from the experimental settings, rather than an average of the multiple scans at each setting. Each of these figures present h_{CO2} with respect to mass flux (W) for different pressures, with heat flux

(Q_A) held approximately constant. The pressure is expressed as a ratio P/P_c. The successive figures are for increasing values of heat fluxes. Two trends can be seen on Fig. 5, the lowest heat flux tested. First, h_{CO2} increased as the mass flux increased for all pressures. The anomalous drop in h_{CO2}, on the P/P_c =1.05 curve at 500 kg/(m^{2}s) mass flux, is due to its higher T_b than the other points on the curve (we will demonstrate the effect of T_b in data set 6). The trend of h_{CO2} increasing with W would also occur for a constant property (non-supercritical) fluid. Second, as the pressure increased, h_{CO2} decreased for all values of the mass flux. At this low Q_A, the heat transfer coefficient was highest at the lowest pressure (close to the critical) and at high mass flux, which also corresponded to high Reynolds number.

Examining Figs. 6 and 7 for higher values of the heat flux shows that an increase in W always increased h_{CO2}. As Q_A was increased, a decrease in pressure produced a smaller, yet still significant, increase in h_{CO2}. When several sets of data with the same pressure and differing Q_A are compared, it is seen that increasing the heat flux decreased h_{CO2} when the pressure was low, but had little effect on h_{CO2} when the pressure was high. For a constant property fluid, the heat transfer coefficient would not change as the heat flux varied. Hence the supercritical fluid behaved more like a constant property fluid at the high pressures.

Effect of P/P_c very close to 1.0. In data set 5, we varied P/P_c from 1.0034 to 1.125 at approximately constant flow rate, for four values of Q_A. The results for h_{CO2} are plotted in Fig. 8. For high Q_A, a modest increase in h_{CO2} was obtained for decreasing the pressure. For the lowest Q_A, h_{CO2} approximately doubled as P/P_c decreased from 1.12 to 1.01. Except for the data at P/P_c around 1.12, $T_b > T_m$ for all the points plotted on the figure. The slight decrease in h_{CO2} at the lowest pressure is less than the experimental uncertainty.

Effect of T_b close to T_m. In data set 6, we varied $T_b - T_m$ from about -3 °C to +3 °C at constant pressure and approximately constant flow rate. Fig. 9 shows the results for four values of Q_A. For all values of Q_A, h_{CO2} reached a peak when $T_b - T_m = 0$ °C, although the peak was much larger for the low heat flux. This figure also shows an important relationship between the heat flux and the operating temperature: for $T_b - T_m > -1$ °C, *increasing* Q_A caused h_{CO2} to *decrease*, whereas for $T_b - T_m < -1$ °C, *increasing* Q_A caused h_{CO2} to *increase*. This change in behavior with temperature was not observed when the carbon dioxide was heated instead of cooled; for that configuration, lower heat flux always improved the heat transfer coefficient (Olson, 1999).

Effect of W and Q_A with $T_b < T_m$. Fig. 10 plots the results of the experiments from data set 7 where we varied W and Q_A at $P/P_c = 1.05$ and $T_b - T_m \approx -4$ °C. As we observed from data set 6, h_{CO2} increased as Q_A increased. This occurred throughout the range of flowrates tested. h_{CO2} also increased as W increased.

4.2 Comparisons of the data with predictions from the literature

The experimental results for the Nusselt number were compared to several correlations for turbulent flow from the literature, developed for either constant property flow or supercritical flow. The first was the constant property correlation of Petukhov as modified by Gnielinski (1976). According to Rohsenow *et al.* (1985), this is the most accurate correlation for constant property turbulent flow in a tube. It has a stated accuracy of 10 % over $2300 < Re < 5 \times 10^6$ and

$0.5 < Pr < 2000$:

$$Nu_{CPb} = \frac{f/2\,(Re-1000)Pr}{1+12.7\left(f/2\right)^{1/2}\left(Pr^{2/3}-1\right)}\left[1+(D/L)^{2/3}\right]. \tag{11}$$

The term in the brackets accounts for entry length effects. The fluid properties were evaluated at the T_b. The friction factor, f, is given by the Kármán-Nikuradse correlation:

$$\frac{1}{\sqrt{f}} = 4.0\log\left(Re\cdot\sqrt{f}\right)-0.4 \quad . \tag{12}$$

A common supercritical correlation is the one proposed by Krasnoshchekov and Protopopov (1966). Jackson and Hall (1978) recommended this correlation for both carbon dioxide and water, after they extensively reviewed a number of supercritical correlations in the literature. The correlation was meant to apply to heating of supercritical fluids when the wall heat flux was constant. We earlier found (Olson and Allen, 1998) that this correlation could be applied to the test section of the present work undergoing convective heating boundary conditions, and it was hoped it could also be applied to convective cooling boundary conditions to have a "universal" correlation. This correlation accounts for property gradients between the core fluid and the wall by applying a density ratio and a specific heat ratio to the constant property correlation (Eq. 11):

$$Nu_{SCb} = Nu_{CPb}\left(\frac{\rho_w}{\rho_b}\right)^{0.3}\left(\frac{\overline{c_p}}{c_{p,b}}\right)^{n} , \tag{13}$$

$$\overline{c_p} = \frac{i_w - i_b}{T_w - T_b} \quad .$$

The subscript "w" signifies the variable is evaluated at the conditions of the wall; the subscript "b" signifies an evaluation at the bulk flow conditions of the CO_2. The wall temperature was calculated from the linear addition of the heat transfer modes (Eq. (2)). The exponent n in Eq. 13 depends on T_w, T_b, and T_m:

if $T_w/T_m < 1.0$ or if $T_b/T_m => 1.2$: $\quad n = 0.4$,

if $T_b/T_m < 1.0 <= T_w/T_m$: $\quad n = 0.4 + 0.18\left(\frac{T_w}{T_m}-1\right)$,

if $T_w/T_m => 1.0$ and $1.0 < T_b/T_m < 1.2$: $\quad n = 0.4 + 0.18\left(\frac{T_w}{T_m}-1\right)\left[1-5\left(\frac{T_b}{T_m}-1\right)\right]$. (14)

For our data, n always equaled 0.4, since $T_w/T_m < 1.0$. As noted by Pitla *et al.* (1998), one of the

few correlations in the literature for supercritical cooling is that proposed by Krasnoshchekov *et al.* (1969), which was developed from experimental cooling data on carbon dioxide in a horizontal tube, 2.22 mm ID and 150 mm long ($L/D = 67.6$). The pressure for their experiments was 8.0 to 12.0 MPa. Their correlation is:

$$Nu_{SCw} = Nu_{CPw}\left(\frac{\rho_w}{\rho_b}\right)^p\left(\frac{\overline{c_p}}{c_{p,w}}\right)^q . \tag{15}$$

Note the similarity in form to Eq. 13. Nu_{CPw} is a constant property correlation of exactly the same form as Eq. 11, but with all fluid properties evaluated at the wall temperature. The exponent p varies from 0.3 to 0.8, and is a function of P/P_c. The exponent q is a function of both the specific heat ratio and P/P_c, and varies from 0.4 to 1.0. The reader is referred to Krasnoshchekov *et al.* (1969) for the p and q functions.

Table 3 compares the experimental Nusselt number, Nu_{meas}, to that predicted by the two constant property correlations (Nu_{CPb}, Nu_{CPw}) and the two supercritical correlations (Nu_{SCb}, Nu_{SCw}). For each data set, the extremes in the deviation between the predicted and measured value, along with the average and standard deviation of the difference, are given for each data set. The combined standard uncertainty in the measurement is given for comparison. For $T_b > T_w$, (data sets 1 to 4), both constant property correlations under-predicted the measured heat transfer, with the wall-based correlation performing worse than the bulk fluid correlation. The amount of under-prediction was more than the combined standard uncertainty of the measurement. The wall-based supercritical cooling correlation, Nu_{SCw}, over-predicted the measured values, also by more than the experimental uncertainty.

Remarkably, the Nu_{SCb}, developed for supercritical *heating*, predicted the data for *cooling* when $T_b > T_m$. Figure 11 shows the percent difference between the correlation and measurement plotted against $T_b - T_m$. The difference falls within the 10 % uncertainty band of the measured Nu for $T_b - T_m > 0$. Once $T_b - T_m < 0$, the differences become large. Analyzing 1200 of the 1564 total points where $T_b - T_m > 0$, the average deviation between Nu_{SCb} and Nu_{meas} was –1.5 %, and the standard deviation was 5.3 % (compared to the range of one-sigma combined standard uncertainty in Nu_{meas} of 2.4 % to 10.1%).

For the temperature range of $T_b < T_m$ (data set 7 and some settings from sets 5 and 6), the correlation with the closest agreement to the experimental data was the bulk-based constant property correlation, Nu_{CPb}. It still under-predicted the data by 11 % to 47 %, which was greater than the experimental uncertainty. All of the other correlations also under-predicted the data for $T_b < T_m$. The Nu_{CPb} correlation was unable to predict the effect of the higher heat flux increasing the heat transfer coefficient, and also became worse as the mass flow rate decreased.

Figure 12 shows the percent difference between Nu_{SCb} and Nu_{meas} as a function of pressure ratio, for $T_b - T_m > 0$. Although the differences increased as P/P_c approached 1, they were still within two-sigma of the combined standard uncertainty of the measurement. The correlation can be confidently used over the pressure range we tested.

5. Summary and conclusions

In this work we have measured the heat transfer coefficient in turbulent, supercritical carbon dioxide flowing in a horizontal tube. The carbon dioxide was cooled by water flowing countercurrent in the annular gap outside the tube containing the carbon dioxide. This convective boundary condition is the same as in a heat exchanger in which the supercritical carbon dioxide exchanges heat with another fluid, such as the "gas cooler" in a refrigeration cycle. Very little experimental data exists in the literature for cooling of a supercritical fluid, particularly for tubes of diameters about 1 cm.

Our measurements showed that four parameters influenced the heat transfer coefficient during supercritical cooling: mass flow rate, cooling heat flux, system pressure, and average fluid temperature, T_b (in relation to the pseudocritical temperature, T_m). The heat transfer coefficient always increased with increasing flow rate, as would also be expected for a constant property fluid. Pressures close to the critical produced high heat transfer coefficients, with the heat transfer coefficient decreasing as pressure increased. As T_b was increased from below to above T_m, the heat transfer coefficient increased, reached a peak, and then decreased again. The effect of heat flux on the heat transfer coefficient depended on T_b compared to T_m: for $T_b - T_m < -1$ °C, an increase in Q_A produced higher heat transfer coefficients, while for $T_b - T_m > -1$ °C, an increase in Q_A reduced the heat transfer coefficient. For similar values of these four experimental parameters, the heat transfer coefficient under cooling always exceeded its value with heating (Olson and Allen, 1998; Olson 1999), at times by a factor of two or three.

Several heat transfer correlations from the literature were compared to the measured experimental data. None were found to adequately predict the measurements over the entire range of the experimental parameters. A correlation developed for constant heat flux heating (Eq. 13) predicted the data to within experimental uncertainty when $T_b - T_m > 0$ °C, but under-predicted the data for $T_b - T_m < 0$ °C. This is the same correlation that predicted all the heating data on this same tube. A correlation developed for supercritical cooling (Eq. 15) over-predicted the data for $T_b - T_m > 0$ °C, and under-predicted the data for $T_b - T_m < 0$ °C. Two constant property correlations under-predicted the data for nearly all conditions, although one of them (Nu_{CPb}) had the lowest errors of all for $T_b - T_m < 0$ °C.

All of the correlations were developed for "local" heat transfer measurements, whereas our heat transfer coefficient is defined as an overall measurement (using only the inlet and outlet temperatures of the carbon dioxide). It would be useful to verify whether the heat transfer equations could be integrated from the heat exchanger inlet to the outlet, with the heat transfer coefficient expressed by the correlations, to produce the experimentally measured conditions. This would help determine if the differences expressed in Table 3 are a result of the differing definitions of the heat transfer coefficient, or truly represent the expected fundamentally different physics of the supercritical flow.

6. References

Gallagher, J.S., and Haar, L., 1988, "NIST Standard Reference Database 10: NIST Thermodynamic Properties of Water (STEAM)," U.S. Department of Commerce, NIST.

Gnielinski, V., 1976, "New equations for heat and mass transfer in turbulent pipe and channel flow," *International Chemical Engineering*, Vol. 16, no.2, pp. 359-368.

Hall, W.B., and Jackson, J.D., 1978, "Heat transfer near the critical point," *Proceedings of the 6th International Heat Transfer Conference*, Vol. 6., pp. 377-392.

Jackson, J.D., and Hall, W.B., 1978, "Forced convection heat transfer to fluids at supercritical pressure," in *Turbulent Forced Convection in Channels and Bundles*, Vol. 2, pp. 563-611, NATO Advanced Study Institute.

Krasnoshchekov, E.A., Kureava I.V., and Protopopov, V.S., 1969, "Local heat transfer of carbon dioxide at supercritical pressure under cooling," *Teplofizika Vyosokikh Temperatur*, Vol. 7, no.5, pp. 922-930.

Krasnoshchekov, E.A., and Protopopov, V.S., 1966, "Experimental study of heat exchange in carbon dioxide in the supercritical range at high temperature drops," *Teplofizika Vyosokikh Temperatur*, Vol. 4, no.3, pp. 389-398.

Lorentzen, G., and Pettersen, J., 1993, "A new, efficient and environmentally benign system for car air-conditioning," *International Journal of Refrigeration*, Vol. 16, no. 1, pp. 4-12.

Olson, D.A., 1999, "Heat transfer in supercritical carbon dioxide with convective boundary conditions," *Proceedings of the 20th International Congress of Refrigeration*, IIR/IIF, Sydney.

Olson, D.A., and Allen, D., 1998, "Heat transfer in turbulent supercritical carbon dioxide flowing in a heated horizontal tube," *NISTIR 6234*.

Pitla, S.S., Robinson, D.M., Groll, E.A., and Ramadhyani S., 1998, "Heat transfer from supercritical carbon dioxide in tube flow: a critical review," *HVAC&R Research*, Vol. 4, no. 3, pp. 1-21.

Rohsenow, W.M., and Choi, H., 1961, *Heat, Mass, and Momentum Transfer*, Prentice-Hall, Inc..

Rohsenow, W.M., Hartnett, J.P., and Ganić, E.N., 1985, *Handbook of Heat Transfer Applications*, McGraw-Hill, Inc..

Span, R., and Wagner, W., 1996, "A new equation of state for CO_2 covering the fluid region from the triple point temperature to 1100 K at pressures up to 800 MPa," *Journal of Physical and Chemical Reference Data*, Vol. 25, no. 6, pp. 1509-1596.

Taylor, B.N., and Kuyatt, C.E., 1994, "Guidelines for evaluating and expressing the uncertainty of NIST measurement results," *NIST Technical Note 1297: 1994 Edition.*

Vesovic, V., Wakeham, W.A., Olchowy, G.A., Senger., J.V., Watson, J.T.R., and Millat, J., 1990, "The transport properties of carbon dioxide," *Journal of Physical and Chemical Reference*

Data," Vol. 19, no. 3, pp. 763-808.

Table 1. Summary of test section parameters and experimental conditions.

Inner tube inner diameter: 10.922 mm
Inner tube outer diameter: 12.700 mm
Carbon dioxide tube hydraulic diameter: 10.922 mm
Carbon dioxide flow area: 9.369 x 10^{-5} m^2
Heated tube length: 2.743 m

Outer tube inner diameter: 16.561 mm
Outer tube outer diameter: 19.050 mm
Water annulus hydraulic diameter: 3.8608 mm
Water flow area: 8.873 x 10^{-5} m^2
Heat transfer area: 9.413 x 10^{-2} m^2

Data Set	No. Settings	No. Data Points	Pressure (MPa)	Flow Rate (kg/min)	Cooling (W)	Inlet Temp. (°C)	Outlet Temp. (°C)	T_b-T_m (°C)	ΔT_{LM} (°C)	*Re* at T_b	h_{CO2} (W/(m^{2}K))	Nu_{meas}
1	16	176	8.7	**1.6 to 4.4**	**1780 to 6150**	41.7 to 74.8	29.4 to 39.2	1.2 to 13.7	5.1 to 34.3	123 950 to 291 700	2661 to 9905	716 to 1730
2	21	231	10.4	**1.1 to 4.7**	**1915 to 6220**	49.9 to 76.8	29.3 to 46.2	1.0 to 6.1	6.0 to 34.5	102 480 to 259 720	2670 to 6841	520 to 1192
3	21	231	7.8	**1.5 to 4.0**	**2005 to 5925**	34.9 to 84.5	27.6 to 33.7	0.5 to 24.2	5.4 to 38.3	117 920 to 291 030	2187 to 13 925	789 to 2368
4	21	231	13.0	**1.8 to 4.7**	**2040 to 6120**	61.6 to 88.6	30.6 to 55.5	0.8 to 2.4	7.5 to 39.4	90 330 to 235 810	2201 to 4825	389 to 843
5	21	231	**7.409 to 8.309**	3.2 to 3.5	**1890 to 6000**	32.2 to 40.2	30.5 to 34.4	-1.3 to 2.8	4.6 to 20.1	155 980 to 290 150	7192 to 19 098	1012 to 3080
6	21	232	7.8	2.9 to 3.1	**1960 to 5080**	32.7 to 40.0	26.7 to 33.8	**-3.1 to 3.0**	5.4 to 17.1	108 710 to 257 780	4825 to 11 775	655 to 2034
7	21	232	7.8	**1.8 to 5.0**	**1990 to 5120**	31.6 to 36.4	23.2 to 27.2	-4.3 to –3.4	7.4 to 18.1	63 250 to 176 240	3734 to 8332	503 to 1123

Boldface type indicates the parameters that were varied in the data set.

Table 2. Summary of standard uncertainties for measurements and fluid properties; combined standard uncertainties for calculated parameters.

Parameter	Major Source of Uncertainty	Magnitude of uncertainty
CO_2 mass flow rate	Instrument calibration	0.075 % + 0.34 kg/h
Water mass flow rate	Instrument calibration	0.05 % + 0.082 kg/h
Fluid temperature	Instrument calibration	0.025 °C
CO_2 absolute pressure	Instrument calibration	2070 Pa
CO_2 differential pressure	Instrument calibration	43 Pa
Water absolute pressure	Instrument calibration	2600 Pa
Water differential pressure	Instrument calibration	430 Pa
CO_2 specific enthalpy and specific heat	Equation of state	2 %
CO_2 viscosity and thermal conductivity	Function accuracy	2 %
Heat balance error, all settings	Temperature measurement, CO_2 specific enthalpy function	2.1 % to 19.7 %
Heat balance error, exclude 12 settings where inlet and outlet CO_2 temps within 0.2 °C of T_m	Temperature measurement, CO_2 specific enthalpy function	2.1 % to 4.7 %
Water heat transfer coefficient	Curve fit to NIST calibration data	4.0 % to 5.1 %
CO_2 heat transfer coefficient	Water heat transfer coefficient	1.3 % to 9.8 %
CO_2 Nusselt number	CO_2 heat transfer coefficient, thermal conductivity	2.4 % to 10.1 %
CO_2 Reynolds number	CO_2 viscosity	2.0 % to 2.5 %
CO_2 Prandtl number	Temperature measurement, CO_2 specific heat	3.5 % to 7.7 %

Multiplying the Table values by a coverage factor of 2 will yield a 95 % confidence interval.

Table 3. Comparison of the Nusselt number predicted by four correlations to measured values.

Data Set	No. Data Points	UNu_{meas}	Nu_{CPb} (Constant Property, T_b)				Nu_{SCb} (Supercritical heating, T_b)				Nu_{CPw} (Constant Property, T_w)				Nu_{SCw} (Supercritical cooling, T_w)			
			Ave. Dev.	Std. Dev.	Max. Dev.	Min. Dev.	Ave. Dev.	Std. Dev.	Max. Dev.	Min. Dev.	Ave. Dev.	Std. Dev.	Max. Dev.	Min. Dev.	Ave. Dev.	Std. Dev.	Max. Dev.	Min. Dev.
1, all	176	2.5 to 6.2	-17.0	20.1	-1.3	-43.0	-0.6	5.4	9.8	-10.7	-31.9	36.1	-6.2	-50.0	33.8	45.6	120.0	-6.9
2, all	231	2.5 to 4.8	-10.1	10.5	-3.8	-14.7	-3.0	4.7	7.0	-9.7	-27.0	28.2	-14.2	-38.4	23.7	30.0	77.4	-3.2
3, all	231	2.4 to 6.8	-31.7	33.8	-12.8	-52.5	1.6	6.1	14.5	-9.6	-48.7	52.5	26.6	-61.7	29.7	32.2	52.8	0.9
4, all	231	2.4 to 3.8	-5.7	6.1	-1.4	-11.1	-0.5	2.1	3.8	-4.5	-16.0	17.3	-5.8	-29.0	21.6	24.5	45.6	4.5
5, all	231	4.2 to 10.1	-24.3	32.8	22.0	-54.0	-9.1	12.5	6.5	-31.8	-61.4	61.7	-45.7	-69.8	2.0	11.6	22.7	-26.9
5, $T_b>T_m$	187	4.8 to 10.1	-28.9	36.2	22.0	-54.0	-5.8	7.7	6.5	-13.5	-63.4	63.6	-56.4	-69.8	6.1	9.4	22.7	-4.0
6, all	232	3.9 to 6.9	-20.2	36.5	61.1	-46.7	-16.3	26.1	9.3	-50.6	-47.9	57.2	86.9	-63.0	-5.8	32.9	40.7	-52.7
6, $T_b>T_m$	144	4.2 to 6.9	-12.5	38.1	61.1	-46.7	-1.1	4.1	9.3	-8.6	-43.4	58.0	86.9	-62.6	17.3	23.1	40.7	-10.8
7, all	232	3.4 to 4.8	-31.3	33.5	-11.1	-47.4	-36.4	38.3	-15.8	-52.7	-48.0	49.3	-27.8	-63.4	-38.5	40.2	-18.2	-54.5
All, $T_b>T_m$	1200	2.4 to 10.1	-17.6	26.1	61.1	-54.0	-1.5	5.3	14.5	-13.5	-37.4	44.3	86.9	-69.8	22.4	29.5	120.0	-10.8

All comparisons are $Nu_{pred}/Nu_{meas} - 1$ (%), where Nu_{pred} is the Nusselt number predicted by the correlation. UNu_{meas}, the combined standard uncertainty, is also given in %.

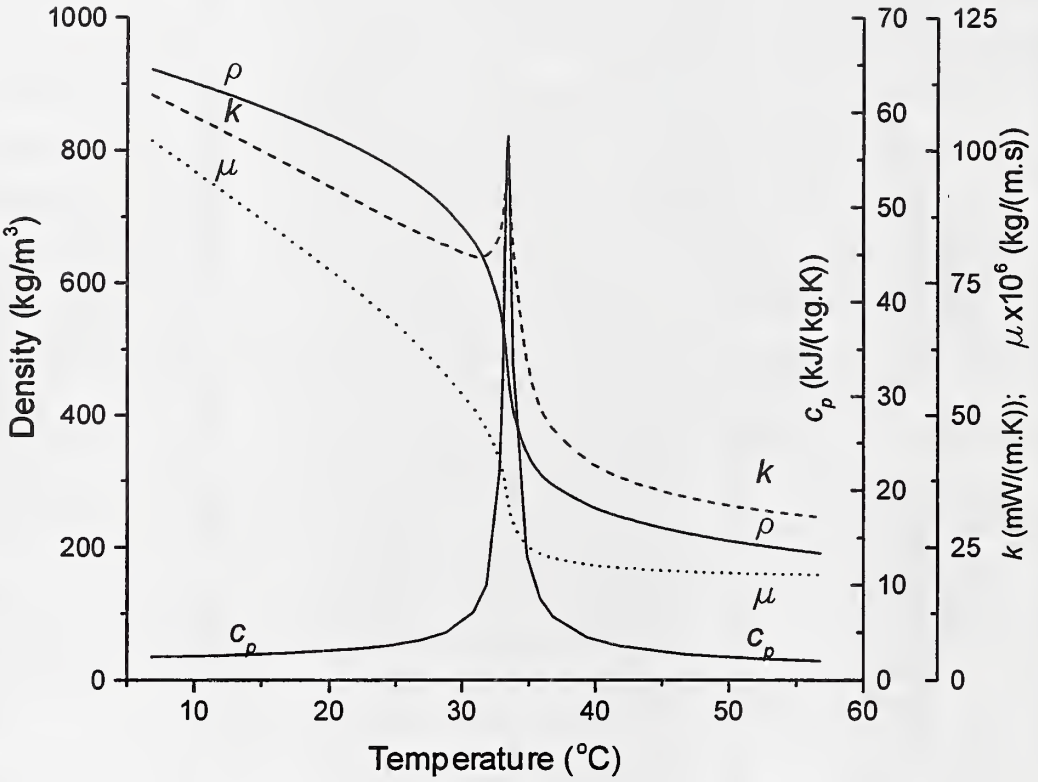

Figure 1. Properties of carbon dioxide on the 7.8 MPa isobar from 5 °C to 55 °C.

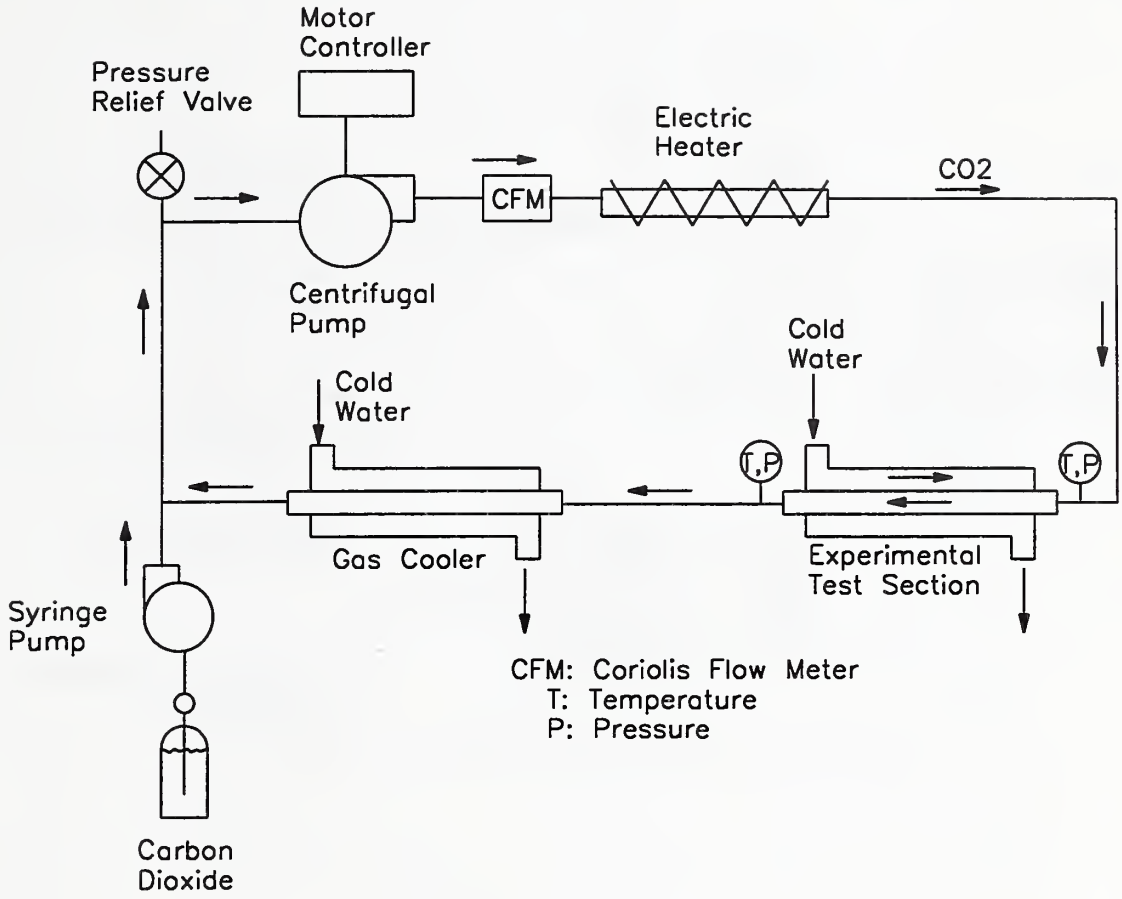

Figure 2. Carbon dioxide flow loop of the NIST supercritical heat transfer facility.

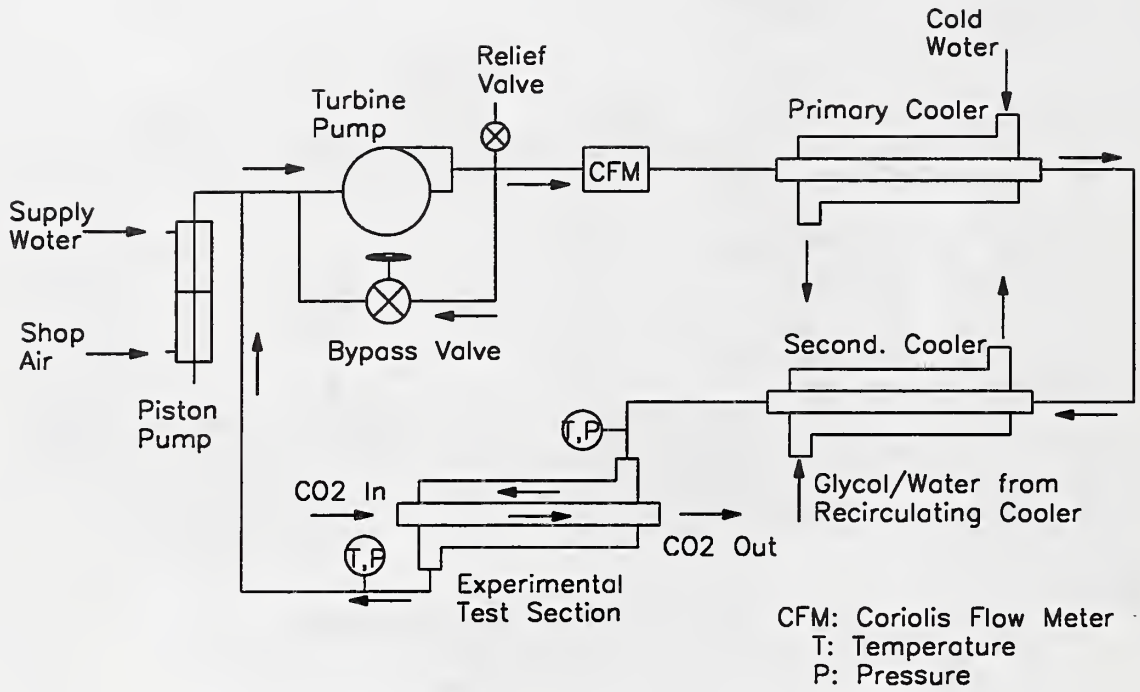

Figure 3. Water flow loop of the NIST supercritical heat transfer facility.

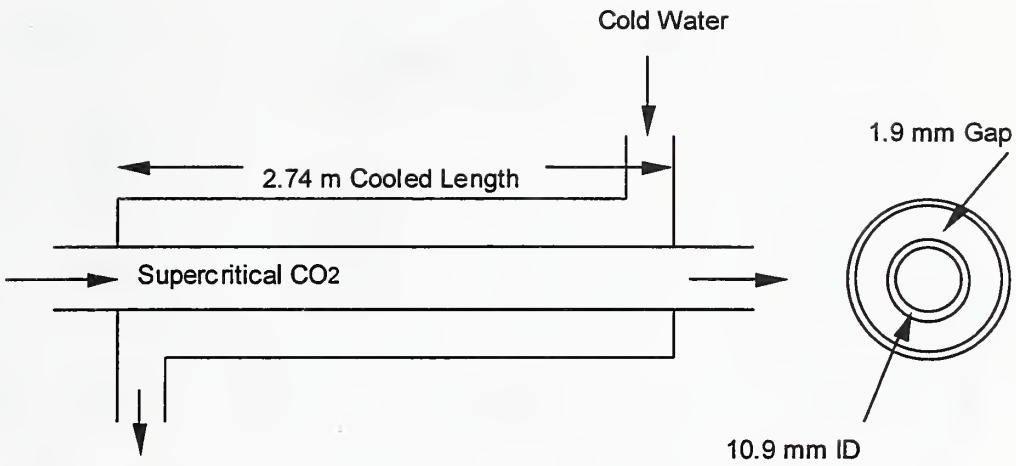

Figure 4. Counterflow heat exchanger test section.

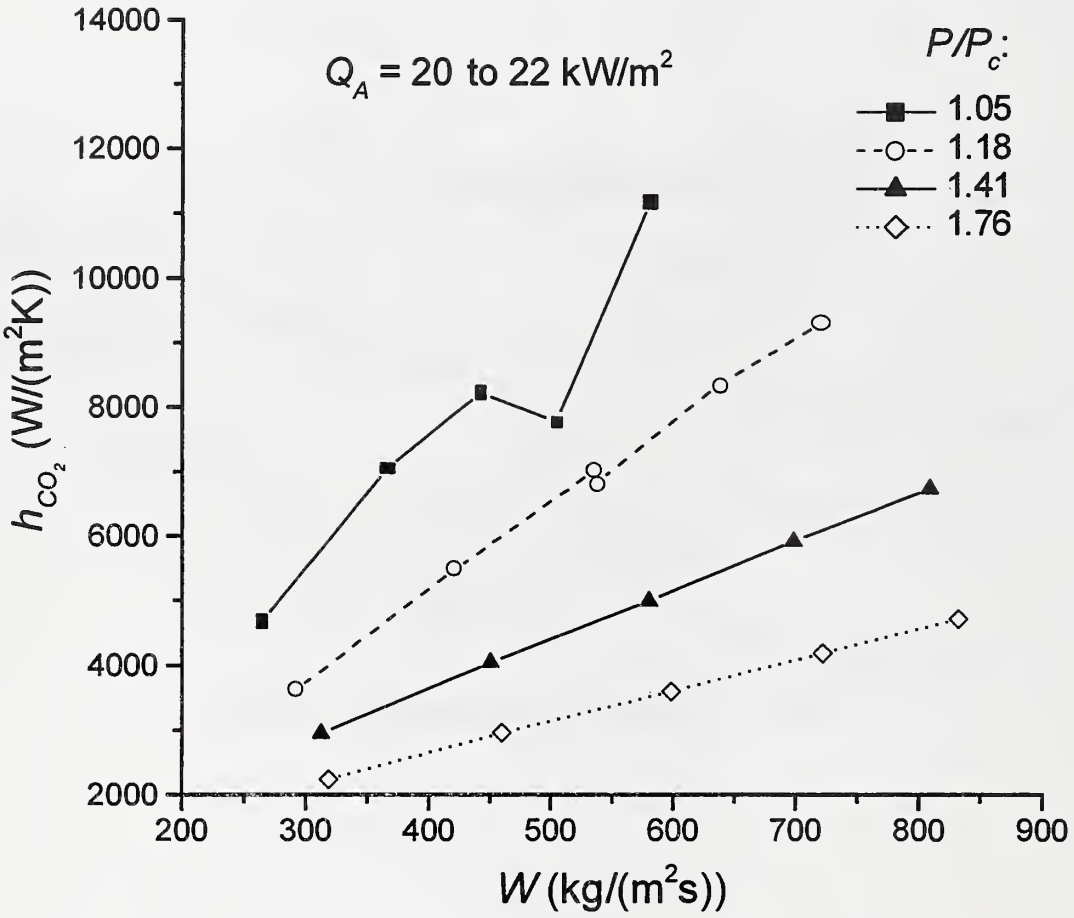

Figure 5. CO_2 heat transfer coefficient (h_{CO2}) as a function of mass flux (W) for several values of pressure (P/P_c) at a heat flux (Q_A) of 20 kW/m^2 to 22 kW/m^2. $T_b > T_m$.

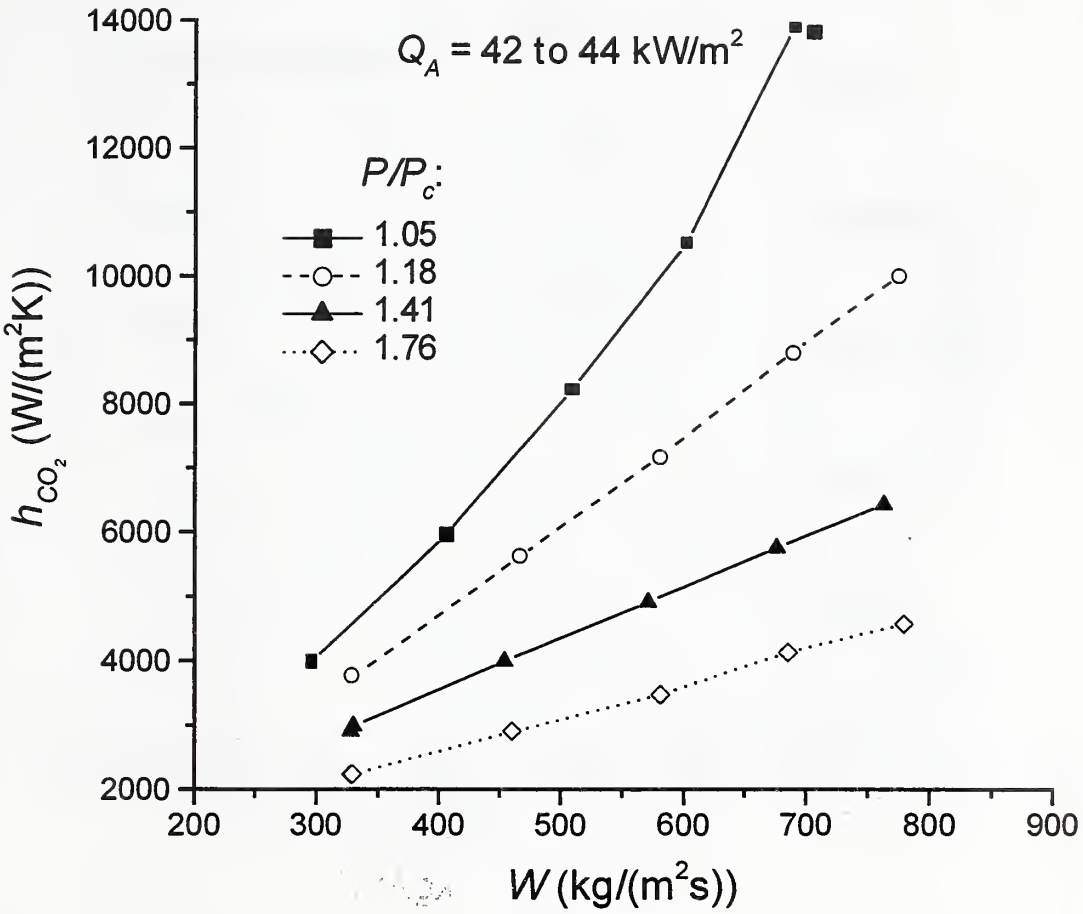

Figure 6. CO_2 heat transfer coefficient (h_{CO2}) as a function of mass flux (W) for several values of pressure (P/P_c) at a heat flux (Q_A) of 42 kW/m^2 to 44 kW/m^2. $T_b > T_m$.

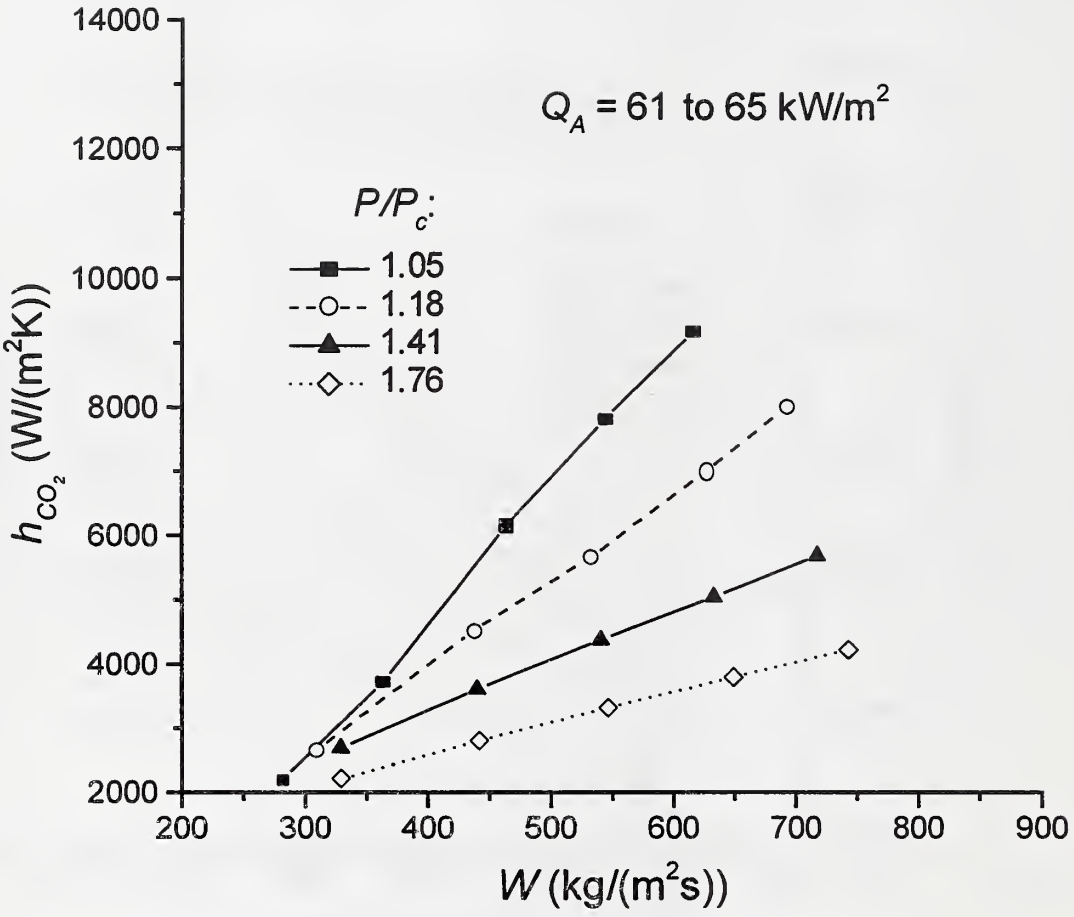

Figure 7. CO_2 heat transfer coefficient (h_{CO2}) as a function of mass flux (W) for several values of pressure (P/P_c) at a heat flux (Q_A) of 61 kW/m^2 to 65 kW/m^2. $T_b > T_m$.

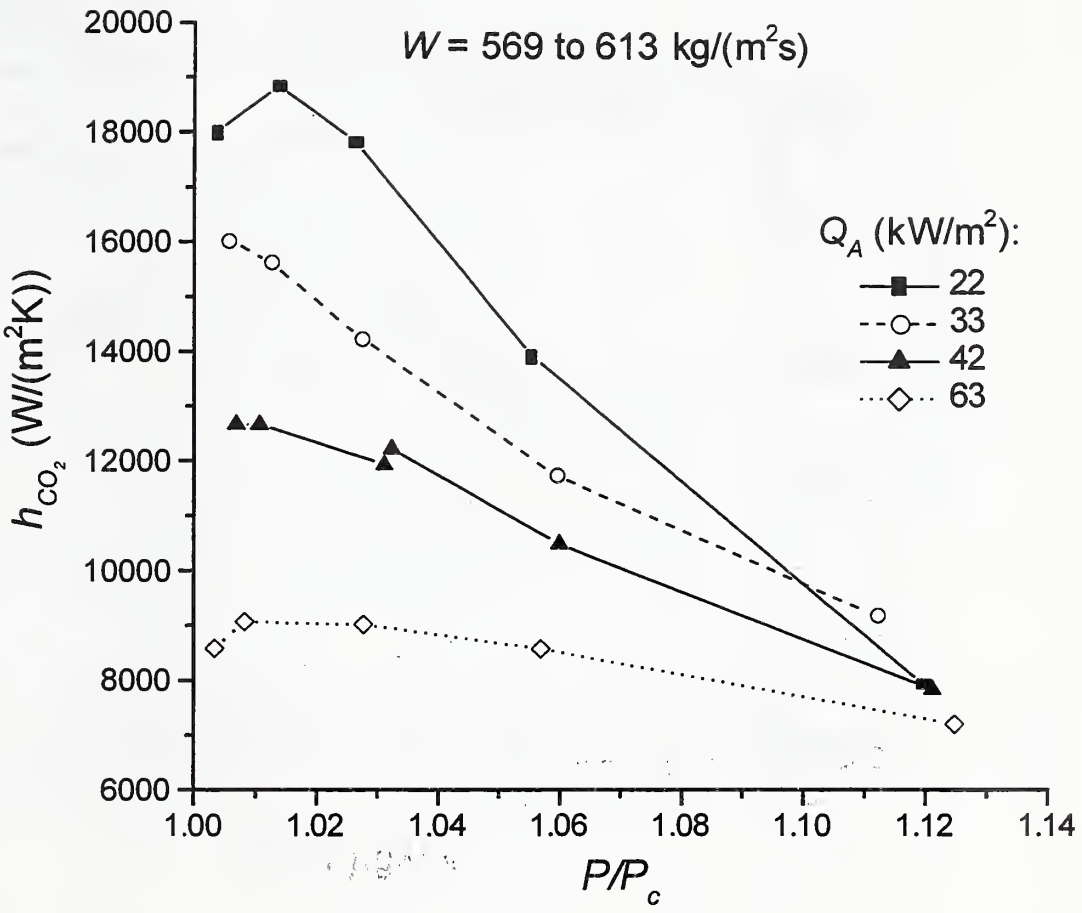

Figure 8. CO_2 heat transfer coefficient (h_{CO2}) as a function of pressure (P/P_c) for several values of heat flux (Q_A) at mass flux (W) of 569 kg/(m^{2}s) to 613 kg/(m^{2}s).

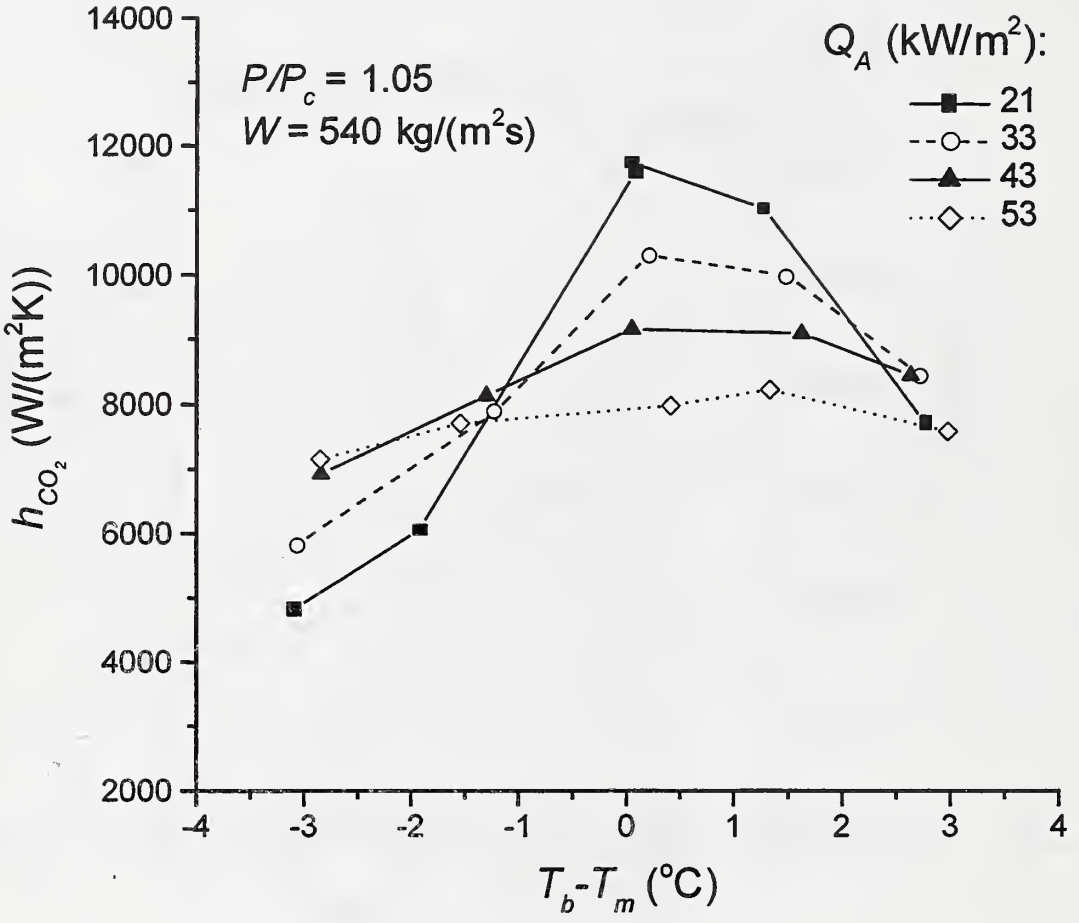

Figure 9. CO_2 heat transfer coefficient (h_{CO2}) as a function of bulk-to-pseudocritical temperature difference ($T_b - T_m$) for several values of heat flux (Q_A). Pressure (P/P_c) of 1.05 and mass flux (W) of 540 kg/(m^{2}s).

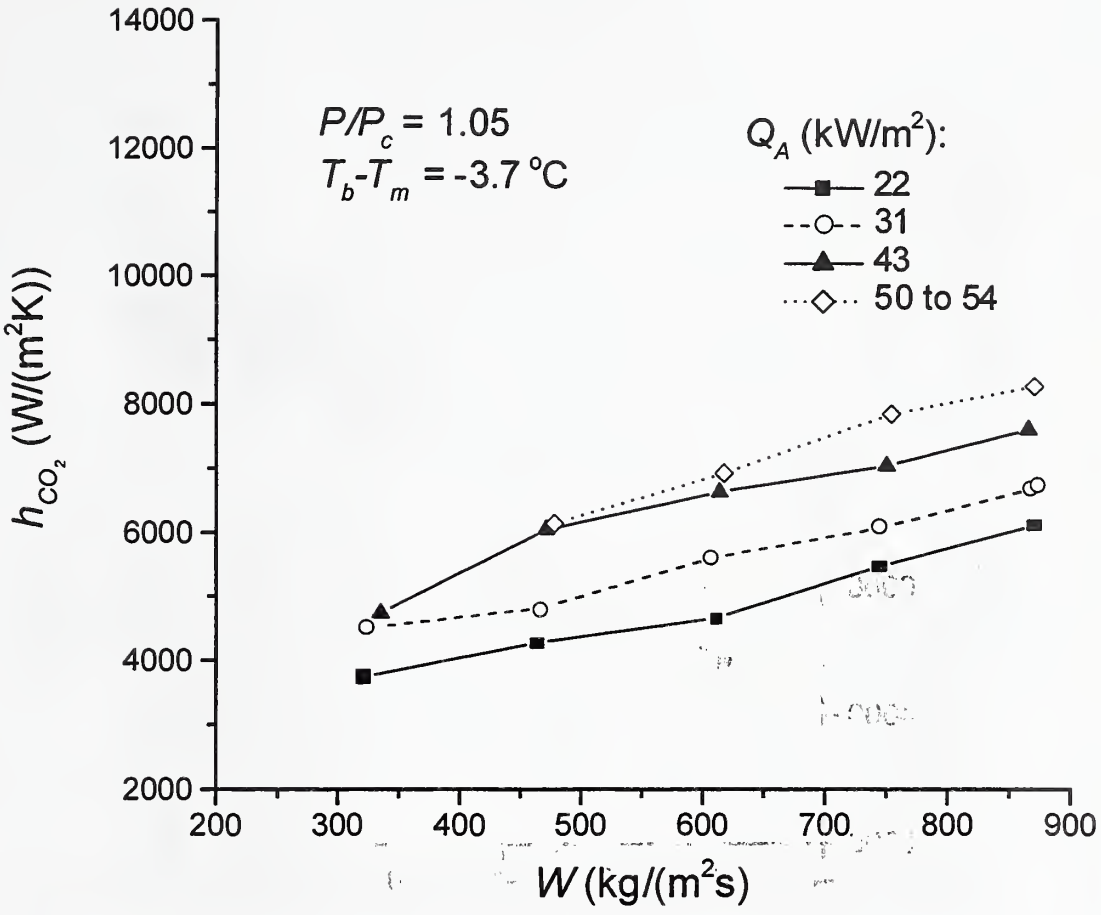

Figure 10. CO_2 heat transfer coefficient (h_{CO2}) as a function of mass flux (W) for several values of heat flux (Q_A). Pressure (P/P_c) of 1.05 and $T_b < T_m$.

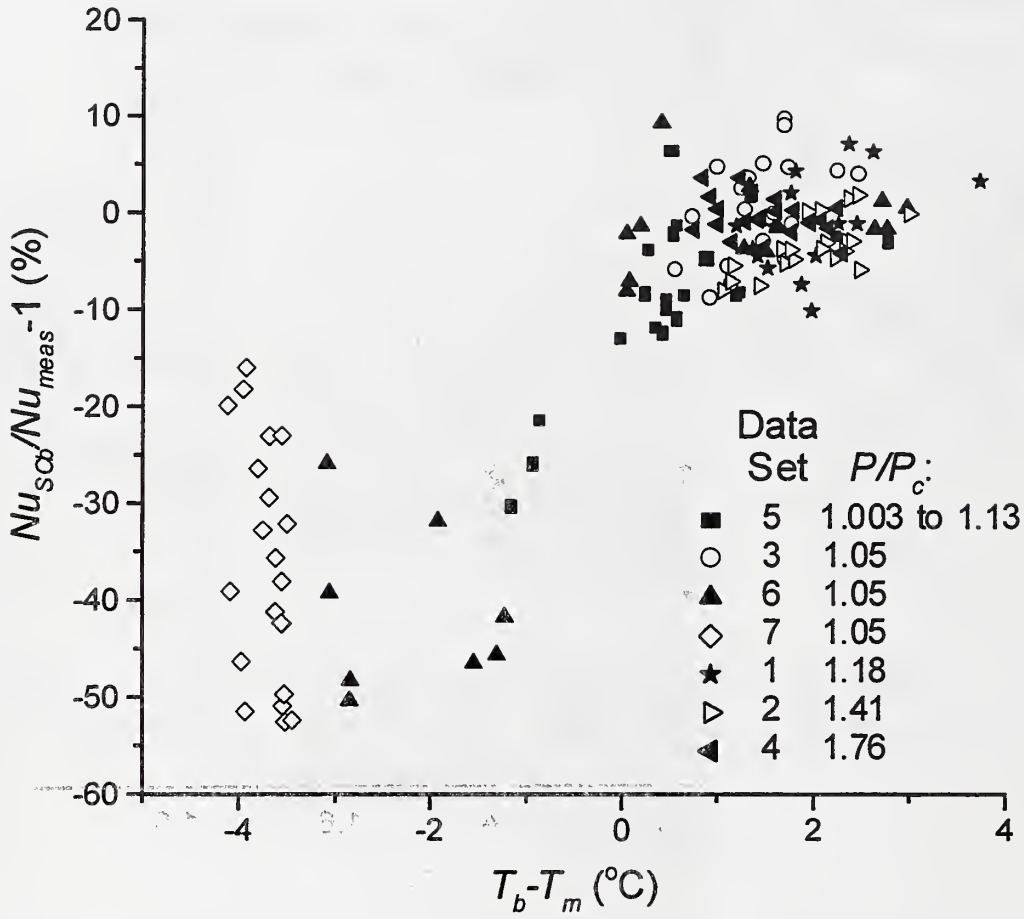

Figure 11. Difference in Nusselt number between Nu_{SCb} correlation and Nu_{meas} as a function of bulk-to-pseudocritical temperature difference ($T_b - T_m$).

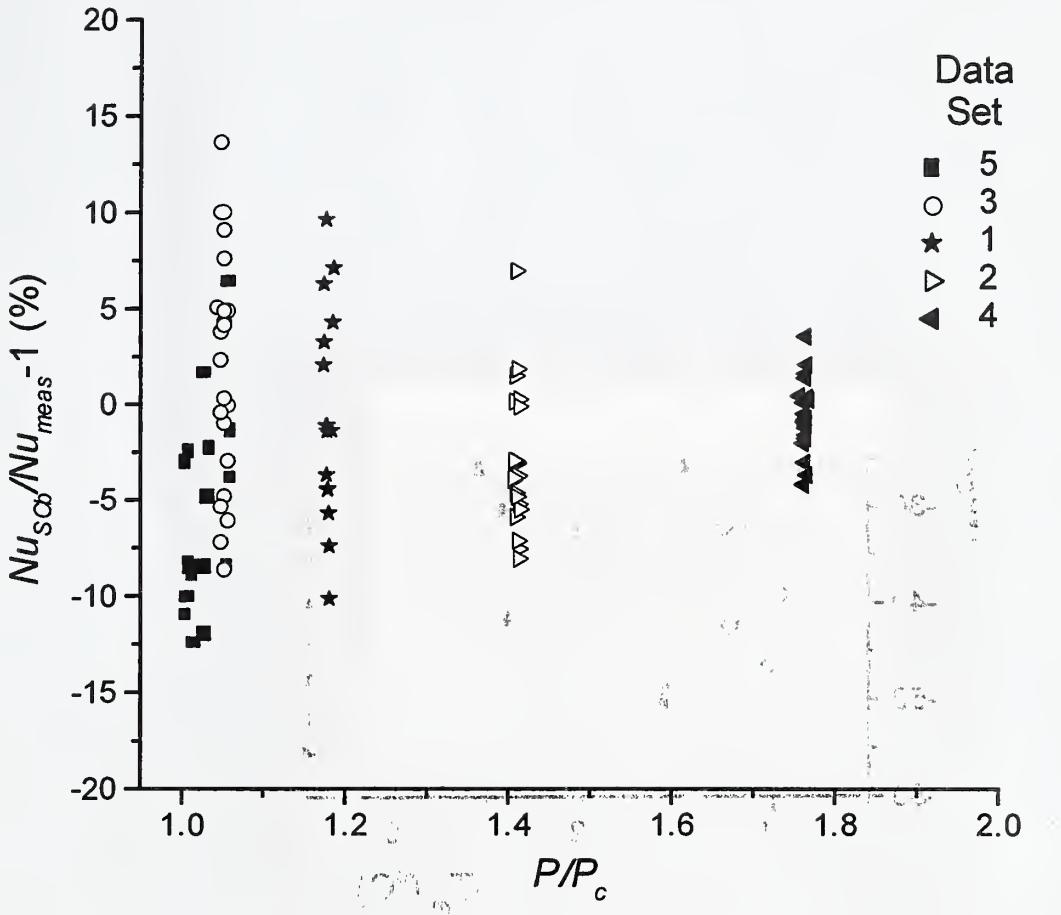

Figure 12. Difference in Nusselt number between Nu_{SCb} correlation and Nu_{meas} as a function of pressure (P/P_c) for $T_b > T_m$.


NISTIR 6496
Olson, 2000
Data Tables
2.0 MB
FORMATTED
FORMATTED
IBM • 1.44 MB
2HD
Primaris